Photoisomerization of Disperse Red 1 Studied with Transient Absorption Spectroscopy and Quantum Chemical Calculations

Mirosława Poprawa-Smoluch, Jacob Baggerman, Hong Zhang, Huub P. A. Maas, Luisa De Cola,† and Albert M. Brouwer*

Van't Hoff Institute for Molecular Sciences, University of Amsterdam, Nieuwe Achtergracht 129, 1018 WS Amsterdam, The Netherlands

Received: September 2, 2005; In Final Form: August 21, 2006

The photoisomerization of the push−pull substituted azo dye Disperse Red 1 is studied using femtosecond time-resolved absorption spectroscopy and other spectroscopic and computational techniques. In comparison with azobenzene, the $\pi\pi^*$ state is more stabilized by the effects of push−pull substitution than the $n\pi^*$ state, but the latter is probably still the lowest in energy. This conclusion is based on the kinetics, anisotropy of the excited state absorption spectrum, the spectra of the ground states, and quantum chemical calculations. The $S_1(n\pi^*)$ state is formed from the initially excited $\pi\pi^*$ state in <0.2 ps, and decays to the ground state with time constants of 0.9 ps in toluene, 0.5 ps in acetonitrile, and 1.4 ps in ethylene glycol. Thermal isomerization transforms the *Z* isomer produced to the more stable *E* isomer with time constants of 29 s (toluene), 28 ms (acetonitrile), and 2.7 ms (ethylene glycol). The pathway of photoisomerization is likely to be rotation about the N═N bond. Quantum chemical calculations indicate that along the inversion pathway ground and excited state energy surfaces remain well separated, whereas rotation leads to a region where conical intersections can occur. For the ground-state *Z* to *E* isomerization, conclusive evidence is lacking, but inversion is more probably the favored pathway in the push−pull substituted systems than in the parent azobenzene.

Introduction

Azobenzenes (ABs) are considered very promising compounds for data storage and other photonic applications.[1] This is due to their fast and reversible photoisomerization (Scheme 1) and the fact that *E* and *Z* isomers differ substantially in their physical properties (volume, dipole moment, etc.). In the ground state the *E* isomer is thermodynamically more stable and the *Z* isomer produced by photoisomerization can undergo thermal reverse isomerization.

The present study of the azobenzene derivative *N*-ethyl-*N*-(2-hydroxyethyl)-4-(4-nitrophenylazo)aniline (Disperse Red 1, DR1; see Scheme 1), is motivated by the role of this dye in light-induced matter migration.[1,2] Although its application in photoinduced surface patterning of polymer films is well-known, the basic photophysical characterization of DR1 is far from complete.[3,4] In the present paper we describe our studies of the dynamics of DR1 in three different solvents. We will show that photoexcitation leads to very short-lived intermediates which decay to the ground state in ca. 1 ps, and the formation of the *Z* isomer as a transient photoproduct, which reverts to the *E* isomer on a time scale of milliseconds to seconds, depending on the solvent properties. In a subsequent paper we will investigate the dynamics of DR1 covalently linked to a sol−gel material.[2,5]

DR1 belongs to the group of push−pull ABs, in which the AB unit is substituted with an electron-donating group in one benzene ring and an electron-withdrawing group in the other. Push−pull ABs have a permanent dipole moment, in contrast

SCHEME 1

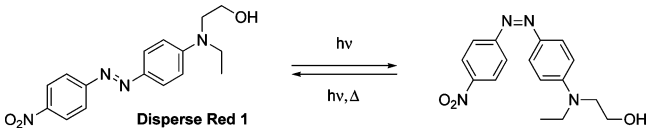

to the nonpolar *E*-AB. The dipole moment is even larger after excitation of the molecule to its $\pi\pi^*$ excited state. The electronic states of push−pull ABs differ substantially from those of the unsubstituted AB. In the latter the lowest excited state is a nonpolar $n\pi^*$ state, which is responsible for a weak absorption in the visible range of the spectrum (ca. 440 nm), which is well separated from the stronger $\pi-\pi^*$ absorption near 320 nm. In the push−pull derivatives a strong $\pi-\pi^*$ absorption with charge-transfer (CT) character is a dominant feature in the visible spectrum, and the $n-\pi^*$ transition is hidden by this strong band. Because of the permanent dipole moment of the ground state and the charge-transfer character of the transition, the absorption band shows a positive solvatochromism.[6,7] Another typical feature of push−pull ABs is that the thermal $Z \rightarrow E$ isomerization is much faster than that for AB, and strongly solvent dependent. As for AB, isomerization may occur via twisting of the N═N double bond, or inversion at one of the nitrogen atoms.[8−10]

While the kinetics and mechanism of photoisomerization of the parent AB have been extensively studied, studies on its push−pull derivatives have been reported by only a few groups. Schmidt et al.[11] reported femtosecond time-resolved fluorescence and transient absorption studies on 4-nitro-4′-(dimethylamino)-azobenzene (DMANAB) in toluene and proposed a model to explain the photoisomerization kinetics. First, within 100 fs, intermolecular and intramolecular modes adapt very rapidly to the new charge distribution caused by CT excitation and a large-

* Corresponding author. Telephone: +31 20 5255491. Fax :+31 20 5255670. E-mail: A.M.Brouwer@uva.nl.

† Present address: Westfälische Wilhelms-Universität Münster Physikalisches Institut, Mendelstr. 7, D-48149 Münster, Germany.

10.1021/jp054982b CCC: $33.50
Published on Web 10/10/2006

amplitude motion away from the Franck−Condon (F−C) region takes place on the excited-state potential energy surface (PES). Then, a "search" for the conical intersection with the ground state occurs within 1 ps and terminates the excited-state dynamics. The authors assumed that a CT state (of $\pi-\pi^*$ origin) is the lowest excited state since its energy is lowered due to the push−pull substitution while the energy of the $n\pi^*$ state remains practically unaffected. Upon return to the ground-state PES, a part of the excited molecules reverts to the initial *E* form, and the other part undergoes photoisomerization to the *Z* isomer. Schmidt et al. concluded that the strong push−pull substitution does not cause substantial changes in the photoisomerization dynamics of AB, but the data presented were not considered to allow any conclusions on the mechanistic pathway of the photoisomerization. Biswas and Umapathy[12,13] studied the influence of solvent polarity (*n*-hexane and benzene) on molecular structure and isomerization dynamics of DMANAB using resonance Raman spectroscopy. They observed a large influence of solvent polarity. Based on the comparison of the distortions in various vibrations of DMANAB with those of unsubstituted AB, they suggest that isomerization occurs via inversion in benzene and via rotation in *n*-hexane. Hagiri et al.[14] investigated photoisomerization of another push−pull azobenzene derivative, *trans*-(4-methoxyphenylazo)-4′-nitrobenzene (MNAB), upon $S_2 \leftarrow S_0$ excitation in acetonitrile using femtosecond transient absorption spectroscopy. They observed very fast formation of the lowest excited state S_1 within 1 ps and a vibrational cooling of the ground state with a time constant of 5−6 ps. Notably, for this push−pull derivative the lowest excited state is clearly the $n\pi^*$ state, similarly to AB.

While only a few studies have been reported on the kinetics of the photoisomerization of push−pull AB, there is a considerable amount of literature on their thermal isomerization. Since the rate of the thermal $Z \rightarrow E$ isomerization is strongly dependent on the solvent polarity, a rotation mechanism via a dipolar transition state was postulated. However, Asano et al.,[15] based on their high-pressure kinetics studies on DMANAB, postulated that the reaction mechanism changes from inversion in *n*-hexane to rotation in benzene and other relatively polar solvents. An interesting study of solvent effects on the rate of the thermal $Z \rightarrow E$ isomerization and the position of the charge-transfer absorption of the *Z* isomer was reported by Schanze et al.[16] for another strong push−pull azobenzene derivative, 4-nitro-4′-(diethylamino)azobenzene (DEANAB). They found a linear correlation of the rate of isomerization with the position of the CT absorption band in different solvents, indicating that a similar degree of CT exists in the transition state for the isomerization reaction and in the Franck−Condon excited state. Furthermore, based on the unit−slope relationship of ΔG (CT) and E_{max} of DEANAB in the solvents studied, the authors suggested the possibility that the thermal and photochemical isomerization reactions occur via a common intermediate that is accessible via light-induced or thermal excitation of the ground-state dye.

In this paper we report a study on the photoisomerization of DR1 in solvents of different polarities and viscosities using femtosecond transient spectroscopy. The measurements were performed at magic-angle, parallel, and perpendicular geometries of pump and probe beams. Thus, not only the decay of transient absorption intensity but also the decay of its polarization anisotropy was investigated. We have also measured the rates of thermal $Z-E$ isomerization and performed quantum chemical calculations to obtain information on the relevant potential energy surfaces and electronic states. The combined experimental and computational evidence is in favor of the $n\pi^*$ state being the lowest excited state, even in polar solvents. The quantum chemical calculations show that the photoisomerization most probably occurs via rotation about the N═N bond, not by inversion.

Experimental Section

Disperse Red 1 (Standard Fluka) was twice recrystallized from toluene and characterized by NMR and HPLC; its purity was estimated to be >99%. All solvents used were of spectroscopic or HPLC grade (Uvasol, Merck; Aldrich).

Steady state absorption spectra were recorded with a diode-array UV/vis spectrometer, Hewlett-Packard 8453. Fluorescence spectra were measured with a Spex Fluorolog 3 fluorometer (Jobin Yvon).

The femtosecond transient absorption setup was described elsewhere.[17] Briefly, an amplified Ti:sapphire laser system (Spectra-Physics Hurricane) equipped with two optical parametric amplifiers (OPAs) was used to produce an ∼100 fs laser pulse train at a repetition rate of 1 kHz. The probe beam was provided by white light generated by focusing a small amount (20 μJ/pulse) of the fundamental beam (800 nm) on a sapphire plate or on a stirred 2 mm H_2O cell. The probe beam was then focused on the sample. The transmitted light was coupled to the detectors by optical fibers. An Ocean Optics (Si, 2048 px) plug-in card diode array was used for the UV−visible region (200−1100 nm). To probe a homogeneously excited area, the pump beam was focused to an area of ∼0.25 mm^2 and the probing area was kept to ∼0.1 mm^2. The samples used for this measurement were prepared so that the absorbance of DR1 was about 1 in a cuvette of 1 mm thickness. To ensure full thermal recovery of the *E* isomer, before every subsequent excitation the acetonitrile and ethylene glycol samples (recovery time on the order of milliseconds) were continuously stirred during measurement, in a regular cuvette, and a flow cell containing about 100 mL was used in case of the toluene sample (recovery time on the order of seconds).

Global analysis of the transient absorption data was performed using Igor Pro, version 5.0.3.[18] In all cases three or four exponential functions convoluted with a Gaussian function representing the instrumental response were used to fit a data set.[19,20] The width of the Gaussian was fixed at the best value obtained from the fits at single wavelengths, and its value was about 200 fs (fwhm) in all cases.

Results

Calculations. To obtain information on the potential energy surfaces and the electronic structures of ground and excited states, quantum chemical calculations were carried out using the B3LYP/6-31G(d) method.[21] Excitation energies were calculated with the time-dependent density functional (TDDFT) method.[22] Calculations were performed for AB and the push−pull derivative DMANAB for both *Z* and *E* isomers in toluene and acetonitrile using the PCM solvent model.[23,24] This push−pull AB derivative is a suitable model compound for DR1, which simplifies calculations. Isovalue surfaces for HOMO−1, HOMO, and LUMO for AB and DMANAB obtained from the calculations are presented in Figure 1.

The highest occupied molecular orbital (HOMO) of DMANAB harbors the lone-pair electrons of the two nitrogen atoms in the azo group (n-electrons); this orbital is quite symmetric, similar to the n-orbital of AB. The highest occupied π orbital (HOMO−

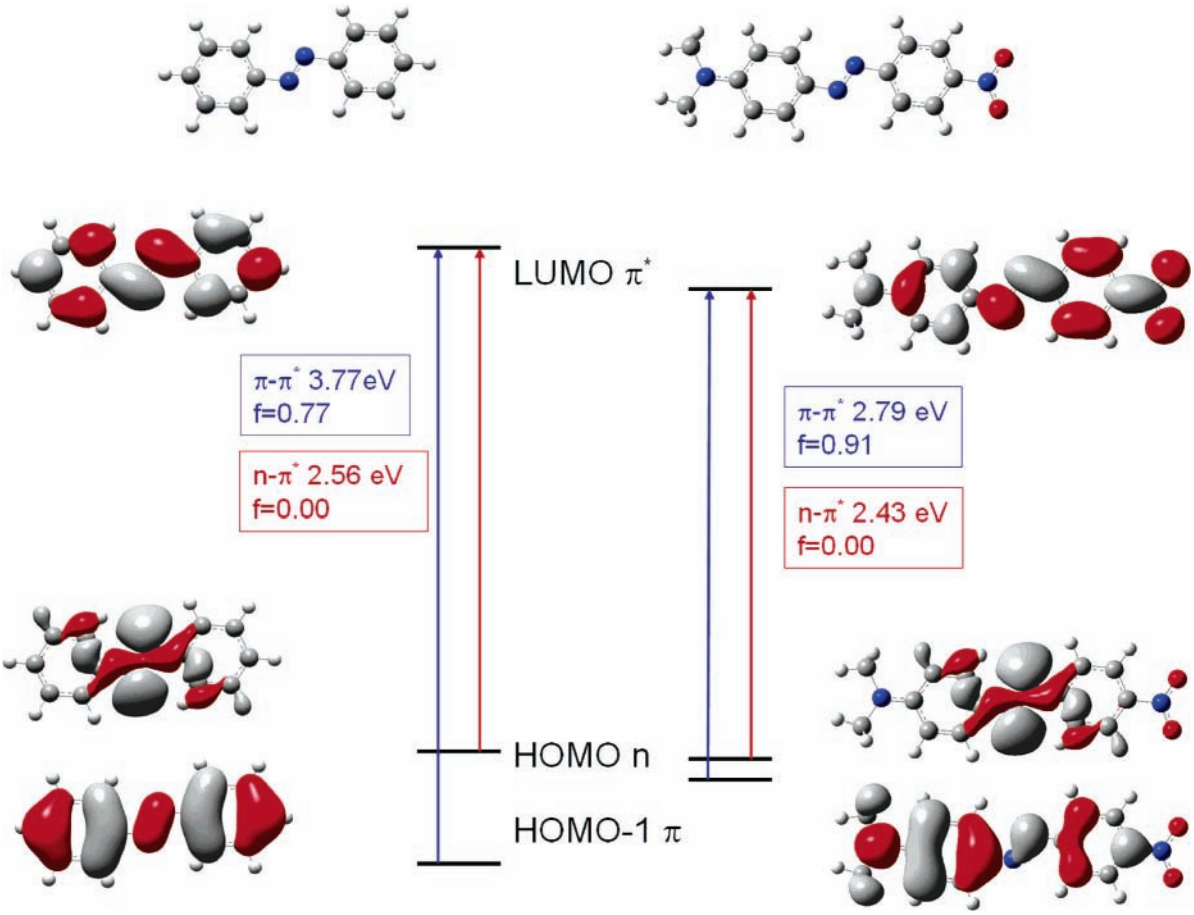

Figure 1. Representation of HOMO−1, HOMO, and LUMO, transition energies, and oscillator strengths for n−π* and π−π* transitions for AB and DMANAB calculated using the TDDFT/B3LYP/6-31G(d) method.

TABLE 1: Absorption Maxima and Molar Absorption Coefficients of DR1 in Different Solvents, and Calculated Excitation Energies (Expressed as λ_{max}) for *E* and *Z* Isomers of 4-(Dimethylamino)-4′-nitroazobenzene

solvent	DR1[a]	*E*-DMANAB[b]	*Z*-DMANAB[b]
none		509 (0); 444 (0.91)	512 (0.15); 415 (0.07)
hexane	446	515 (0); 483 (1.04)	523 (0.23); 433 (0.03)[c]
toluene	473 (31 100)	516 (0); 493 (1.07)	527 (0.25); 437 (0.02)[c]
acetonitrile	487 (40 000)	519 (0.003); 516 (1.03)	545 (0.28); 453 (0.002)
ethylene glycol	502		

[a] Experimental data: λ_{max} in nm and ϵ_{max} ($M^{-1}cm^{-1}$) in parentheses. [b] Computed (TDDFT/B3LYP/6-31G(d)): λ_{max} in nm and oscillator strengths in parentheses. [c] Gas-phase B3LYP geometry used.

1) and π* orbital (lowest unoccupied molecular orbital, LUMO) of DMANAB, in contrast to AB, are asymmetric, being localized more on the electron-donor side and the electron-acceptor side of the π system, respectively. The delocalization of electron density away from the nitrogen atom of the dialkylamino group in the HOMO−1 is responsible for the large ground-state dipole moment (see below, Table 3). Upon π−π* excitation, there is a considerable increase of charge separation, in the same direction as the ground-state dipole moment. This leads to the solvatochromic shift in the absorption spectra, as shown below.

Due to the symmetry selection rules the n−π* transition is forbidden, but it can gain some intensity via coupling with suitable vibrations. The π−π* transition is fully allowed.

Since the transition energies were calculated for ground-state geometries, the energy gaps correspond to experimental values of absorption maxima. For the *E* isomer the values can be directly compared with experiment (Table 1). For the *Z* isomer this is impossible because the experimental spectra are not precisely known due to the impossibility of isolating it in a pure form under the experimental conditions used (room-temperature solution).

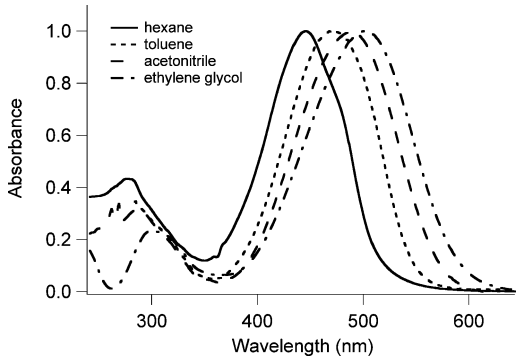

Figure 2. Normalized ground state absorption spectra of DR1 in different solvents.

Absorption Spectra of DR1. Figure 2 shows the absorption spectra of DR1 in different solvents. Photoisomerization of the stable *E* isomer of DR1 to the metastable *Z* isomer was

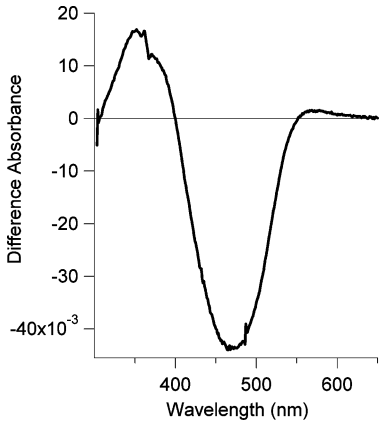

Figure 3. Difference absorption spectrum of DR1 in toluene after flash-induced photoisomerization. The spectrum shows the difference between absorption of the pure *E* isomer and the mixture of *E* and *Z* isomers produced with the light flash.

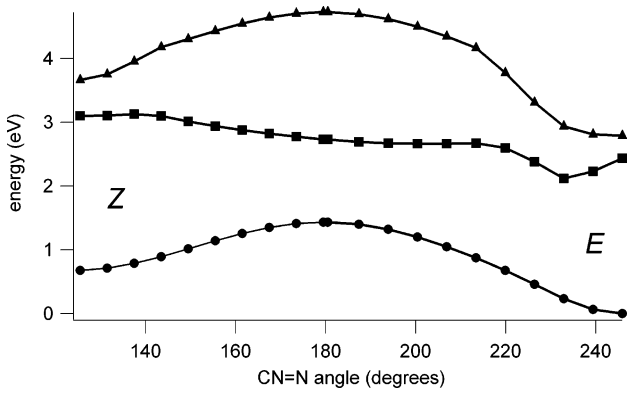

Figure 4. Energies of S_0 of DMANAB along the inversion pathway (full geometry optimization at fixed C−N═N angles) and energies for S_1 and S_2 calculated as TDDFT excitation energies at the ground-state geometries. For the *E* isomer the angle is given as 360° − −(C−N═N).

accomplished using a flash lamp or a nanosecond laser pulse. In the first case the spectral changes were monitored using a diode array spectrophotometer; in the second case a gated CCD detector was used. A representative difference spectrum is shown in Figure 3.

In all solvents examined the absorption spectrum of DR1 consists of two bands: a band in the visible range with a maximum between 420 and 510 nm and a weaker UV band (290−300 nm). This is different for AB, which has three UV−vis absorption bands: one very weak in the visible range assigned to the symmetry forbidden n−π* transition, one strong band in the near UV assigned to the allowed $\pi-\pi$* transition, and another UV $\pi-\pi$* band of higher energy. The difference stems from the fact that strong push−pull substitution induces CT character into the $\pi-\pi$* transitions of AB, as illustrated by the results of our calculations (see Figure 1). This causes a red shift of the $\pi-\pi$* bands. On the other hand, the calculations show that the n−π* transition is less affected by push−pull substitution and, similarly to in AB, is symmetry forbidden. Although the visible band of DR1 originates from the strongly allowed $\pi-\pi$* transition, the nπ* state may still be the lowest excited state. The TDDFT calculations support this state ordering, but we do not consider their accuracy sufficient to allow a firm conclusion. The n−π* transition in DR1 may have some intensity due to vibronic coupling to the higher $\pi-\pi$* transitions via torsional vibrations, as was postulated for AB, but if its absorption coefficient is similar to that in AB it is still much weaker than the $\pi-\pi$* absorption ($\epsilon = (3-4) \times 10^4$ M^{-1} cm^{-1}). The absorption spectra show a positive solvatochromic shift because the ground state has a substantial dipole moment, and the excited state is even more polar, the dipole moments being in the same direction. In the case of ethylene glycol, further stabilization of the excited state by hydrogen bonding may contribute to the red shift.

Commercial samples of DR1 showed weak emission peaking near 670 nm in acetonitrile, but HPLC analysis with simultaneous detection of absorption and emission showed that this emission is due to an impurity. The intensity of emission decreased upon repeated recrystallization.

In Figure 3 the differential absorption spectrum of DR1 in toluene after flash-induced photoisomerization is presented. Unfortunately, the difference absorption spectrum observed corresponds to a mixture of the isomers with an unknown ratio, so the actual spectrum of the *Z* isomer cannot be determined. It is clear, however, that the *Z* isomer absorbs more strongly than the *E* isomer at shorter wavelengths (350−400 nm) and, interestingly, at about 550 nm.

The increase of the absorption around 350 nm with corresponding decrease of the absorption at about 470 nm (the maximum of *E* isomer ground-state absorption) can be explained by the difference in the positions of the absorption maxima of the dominant $\pi-\pi$* bands of the two isomers. The increase of the absorption at about 550 nm can be attributed to the presence of the n−π* transition in the *Z* isomer, which is not hidden under the $\pi-\pi$* band as it is in the *E* isomer. The TDDFT calculations predict the positions of the absorption bands with a small systematic error (Table 1). For the *Z* isomer the energy difference between the two lowest energy transitions is much larger than that for the *E* isomer. This is in agreement with the experimental observation. With the B3LYP method the intensities of the two bands of the *Z* isomer are not correctly predicted; with the Becke Half-and-Half method (as implemented in Gaussian 03) the relative intensities are in better agreement with experiment. It should be realized that although there are still two high-energy occupied orbitals, with the corresponding excited states predominantly described by promotion of one electron to the LUMO, the distinction between n and π orbitals is, in fact, not possible in the nonplanar *Z* isomer.

A similar, but more pronounced, long-wavelength absorption of the *Z* isomer was observed for 4-aminoazobenzene (AAB) in ethanol by Hirose et al.[30] We observe the long-wavelength band only upon photolysis of DR1 in toluene, not in the more polar solvents. This probably because the strong absorption band of the *E* isomer shifts to the red more strongly than the weak transient band. In view of the large energy difference between the two transitions in the *Z* isomer, we can safely assume that the nπ* state is the lowest excited state for the *Z* isomer of DR1 also in acetonitrile and ethylene glycol.

The calculations of the absorption spectra were performed for the energy minimized structures. Interestingly, when the N═N double bond in the *E* isomer is distorted, the energy difference between the two lowest excited states increases markedly. For example, for a small twist of 10°, which requires only 0.65 kcal/mol of distortion energy in the ground state, the energy of the nπ* state decreases relative to that of the $\pi\pi$* state by 2.2 kcal/mol in the isolated molecule, and 5.5 kcal/mol in acetonitrile. Energy curves for the ground state and the lowest excited states along the rotation and inversion pathways are shown in Figures 4 and 5.

Thermal *Z* → *E* Isomerization. Thermal reverse (*Z* → *E*) isomerization of DR1 was monitored using the flash-induced

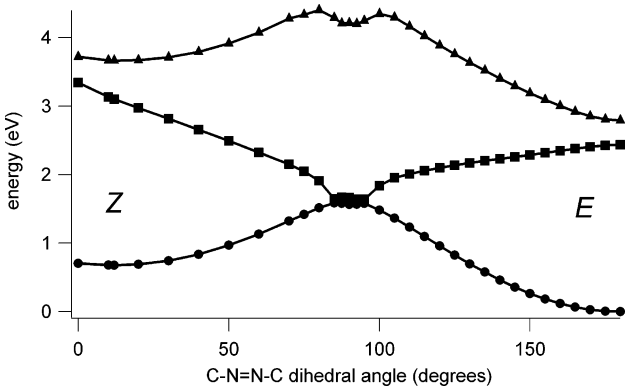

Figure 5. Energies of S_0 of DMANAB along the rotation pathway (C—N═N—C dihedral angle) and energies for S_1 and S_2 calculated as TDDFT excitation energies at the ground-state geometries. In the range 80−100° the C—N═N bond angle was constrained to values near 125° because full geometry optimization in this range of dihedral angles leads to the inversion transition structure.

TABLE 2: Rate Constants of Thermal *Z* → *E* Isomerization of DR1 after Flash-Induced Photoisomerization

solvent	rate constant (s^{-1})
toluene	0.035
acetonitrile	36
ethylene glycol	370

absorption changes, as exemplified in Figure 3. Typically for push−pull AB derivatives, it is substantially faster than for unsubstituted AB and strongly dependent on solvent polarity. The rates of thermal *Z* → *E* isomerization for DR1 in several solvents are collected in Table 2. The rates vary over 4 orders of magnitude with solvent polarity.[16,25] Assuming identical preexponential factors, this amounts to differences in activation energies of 5.5 kcal/mol. For 4-(diethylamino)-4′-nitroazobenzene the activation enthalpies were reported to be 13 and 9.7 kcal/mol in benzene and acetonitrile, respectively.[16] Evidently, the transition structure is considerably more polar than the *Z* isomer.

Computation of Potential Energy Surfaces. The computational comparison of the possible reaction modes, inversion and rotation, is complicated by the fact that the rotation pathway leads through a transition structure in which the N═N bond is effectively broken, leaving two nearly degenerate p-orbitals on the nitrogen atoms occupied with two electrons. Such a singlet biradicaloid configuration cannot be described properly by standard computational methods, which use a single Slater determinant to construct the electronic wave function.[26,27] For the inversion pathway, this problem does not play a role: it only involves a change of hybridization at one of the nitrogen atoms, and orbital degeneracy does not occur.

We have calculated the structures, energies, and electronic properties of the two isomers and the inversion transition structure of DMANAB using the B3LYP/6-31G* methodology. Solvent effects were taken into account using the PCM model.[23,24] The results are listed in Table 3. Molecular structures are shown in Figure 6.

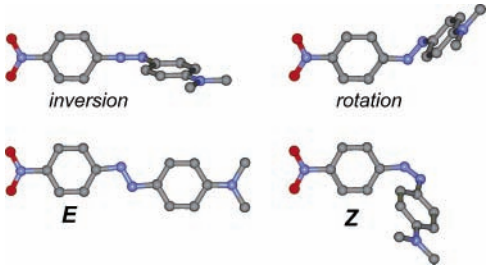

Figure 6. Molecular structures computed for DMANAB. Stable isomers *E* and *Z*, inversion TS, and highest energy structure along the rotation pathway. For clarity, hydrogen atoms have been omitted.

Starting from the *Z* isomer, a smooth reaction path to the inversion transition structure (TS) can be obtained by stepwise increasing the C—N═N angle. In this case the C—N═N—C dihedral angle goes from −11° in the *Z* isomer to 0° near the TS. The nitrophenyl ring rotates smoothly to its final orientation in the TS, in which it is in an orientation perpendicular to that of the rest of the molecule (see Figure 6). For the *E* isomer a smooth reaction pathway can be obtained starting from the TS.

Qualitatively, the solvent effect on the isomerization barrier is reproduced by these calculations, but quantitatively, the agreement is only modest. Earlier calculations by Kikuchi et al.[28] at a considerably lower level of theory (HF/6-31G//HF-STO-3G with a generalized Born solvation model) led to the same conclusion. Remarkably, the results obtained when the rotation reaction path was followed are very similar to the findings of Kikuchi et al.: up to a C—N═N—C dihedral angle of ca. 75° (100° when coming from the *E* isomer), a smooth path is followed, in which minor changes of other geometrical parameters occur following the imposed change of the dihedral angle. Then suddenly the nitrogen inversion coordinate enters into play (at the side of the nitrophenyl ring),[28] and the structure optimizes to the inversion TS by an increase of the C—N═N bond angle to 180°. In this geometry the C—N═N—C dihedral angle is no longer defined. This reaction path was computed for isolated DMANAB, but it was qualitatively the same when a scan of the PES was made and the energies were reevaluated using the PCM model for acetonitrile. Because the dipole moment increases more going toward the pure rotation TS (up to 24 D in acetonitrile, 17 D in the isolated molecule) than in the inversion TS, the minimum energy pathway stays close to the rotation coordinate somewhat longer than in the case of the isolated molecule. A TS for rotation could not be located, but by constraining the C—N═N angle to values of 120−125° structures were obtained which are ca. 4 kcal/mol higher in energy than the inversion TS. Plots of the energies of the ground state, S_1, and S_2 are shown in Figure 5.

For AB, the pure rotation coordinate can be followed, without spontaneous excursion to the inversion TS. This indicates that the likelihood that inversion is a relevant reaction coordinate

TABLE 3: Relative Energies and Dipole Moments of *E*-DMANAB, *Z*-DMANAB, and the Inversion Transition Structure in Isolated Molecules, in Toluene, and in Acetonitrile[a]

	relative energy (kcal/mol)			dipole moment (D)		
structure	isolated	toluene[b]	ACN	isolated	toluene[b]	ACN
E	−15.6	−15.3	−14.1	11.1	12.7	15.5
TS	17.4	16.4	15.7	14.6	16.8	19.4
Z	0[c]	0[d]	0[e]	8.2	9.3	11.1

[a] B3LYP/6-31G(d) with PCM. [b] Geometries optimized for the isolated molecules. [c] Absolute energy −911.210 89 hartree. [d] Free energy in solution −911.207 48 hartree. [e] Free energy in solution −911.206 00 hartree.

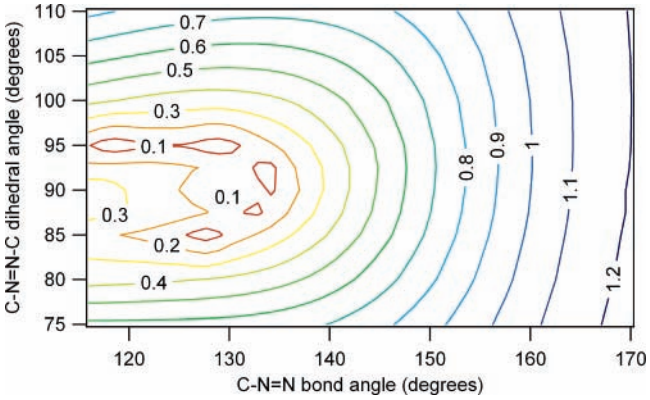

Figure 7. Contour plot of the TDDFT excitation energies $S_0 - S_1$ of DMANAB as a function of the C—N═N angle and the C—N═N—C dihedral angle. A region with low excitation energies ($\Delta E(S_1-S_0) < 0.2$ eV) is found in the range of dihedrals around 90° but not near the inversion transition structure (C—N═N bond angle = 180°).

for thermal isomerization is greater in the case of the push—pull systems than in AB itself.

On the basis of their CASPT2 calculations, Cembran et al. have revived the old idea that the thermal isomerization of AB may involve an intersystem crossing to the lowest triplet state, which is much lower in energy than the singlet biradicaloid in a wide range of dihedral angles around 90°. Also for DMANAB such a reaction path appears feasible.

At present, although our calculations support the feasibility of the inversion reaction coordinate on the ground-state potential energy surface, we cannot exclude that the rotation pathway will turn out to be of lower energy when calculated with a proper multiconfiguration method. It is unfortunately not possible at present to perform CASPT2 calculations with a sufficiently large active space for DMANAB.

TDDFT calculations for geometries with C—N═N—C dihedral angles of 85—95° and C—N═N bond angles in the range 120—135° show very small excitation energies (<0.1 eV), which indicates that a crossing seam between S_0 and S_1 exists in this region of the coordinate space (Figure 7). Although the restricted DFT method is not expected to be able to properly describe the conical intersection structures, which have an open shell character, Fantacci et al. showed that very low TDDFT excitation energies were observed at geometries that were calculated as conical intersections with the CASPT2 method.[29] Moving along the inversion pathway by increasing the C—N═N angle the energy difference between S_0 and S_1 stays large, which strongly supports the idea that for push—pull ABs (as for AB) the pathway for photoisomerization involves rotation, not inversion.

Femtosecond Transient Absorption under Magic-Angle Conditions. Pump—probe spectra of DR1 were measured with pump and probe beams polarized at the magic angle in toluene, acetonitrile, and ethylene glycol. The pump wavelength was chosen in all cases at the short-wavelength side of the low-energy absorption band, so that the bleaching band due to ground-state depopulation in the transient spectrum could be well detected. Control experiments with excitation at longer wavelengths did not reveal any difference in the dynamics. Because of this choice of wavelength of excitation, molecules of DR1 are excited to higher vibrational levels of the $\pi\pi^*$ excited state. In all three solvents the obtained transient spectra are essentially similar (Figure 8). They consist of three distinct bands: a negative band in the range of ground-state absorption (bleaching band), a weak positive band on the red edge of the ground-state absorption, and a strong broad positive band covering much of the visible range, peaking around 700 nm. Each of the three bands exhibits different kinetic behavior (see Figure 9). At very early times, before the maximum of the system response is reached, the spectrum appears to change shape (Figure 8A). This is most pronounced in acetonitrile. The "dip" around 600 nm may be attributed to stimulated emission from the (incompletely relaxed) $\pi\pi^*$ excited state.

The bleaching band does not return to zero amplitude during the measurement time window (1 ns), and its recovery cannot be fitted with a simple exponential rise function. The residual bleaching that is observed can be explained by the fact that the *Z* isomer has a different ground state absorption spectrum than the *E* isomer (see Figure 3). Thus, those molecules that undergo photoisomerization do not contribute fully to the recovery of the ground-state absorption. Therefore the amount of residual bleaching is informative of the relative efficiency of photoisomerization even if the spectral shape and absorption coefficient of the *Z* isomer are unknown.

In all solvents the positive low-energy band peaking near 700 nm decays faster than the high-energy feature near 550 nm. Both bands, however, decay quite rapidly: after about 20 ps there is no differential absorption signal left except the part of the bleaching band due to photoproduct formation. The low-energy band decays monoexponentially with time constants of 0.9, 0.5, and 1.4 ps in toluene, acetonitrile and ethylene glycol, respectively, but in toluene and acetonitrile also a very short rise time (0.13 and 0.22 ps, respectively) is obtained from the single-wavelength fits. In view of the approximate representation of the system response as a Gaussian, the value of the rise time constant is somewhat uncertain. Decay of the band near 550 nm can be fitted with the same constants as the low-energy band (apparently due to the spectral overlap) and one extra component which is longer (several picoseconds, in all solvents). The bleaching band recovery can be fitted very well with all three time constants obtained from fitting the time profiles of the two positive bands.

Subsequently, global fitting was performed on the whole data set using as starting values the three (or two, in the case of ethylene glycol) time constants obtained from single-wavelength analyses. Additionally, in all cases, one constant was used to fit the offset due to the formation of the *Z* isomer. Results of the best global fits are shown in Figure 10. In this way, decay-associated spectra (DAS) and the corresponding time constants were obtained. The values of time constants obtained from the global fits agree very well with those obtained from fitting the single-wavelength decays (see Table 4). DAS obtained from the global fits indicate that decays of both states giving rise to the positive transient absorption bands contribute to the recovery of the ground state. Fairly random residual distributions obtained for all global fits show that the assumed model fits the data well. Small discrepancies obtained for the first hundreds of femtoseconds originate from the fact that spectra are changing slightly in this time range (see Figure 8A).

Polarization Anisotropy of Femtosecond Transient Absorption. Transient absorption spectra of DR1 in toluene and ethylene glycol were also recorded with parallel and perpendicular relative polarizations of the pump and probe beams. From this experiment the value of polarization anisotropy $r(t)$ for transient absorption was calculated according to the relation

$$r = \frac{I_{par} - I_{perp}}{I_{par} + 2I_{perp}} \quad (1)$$

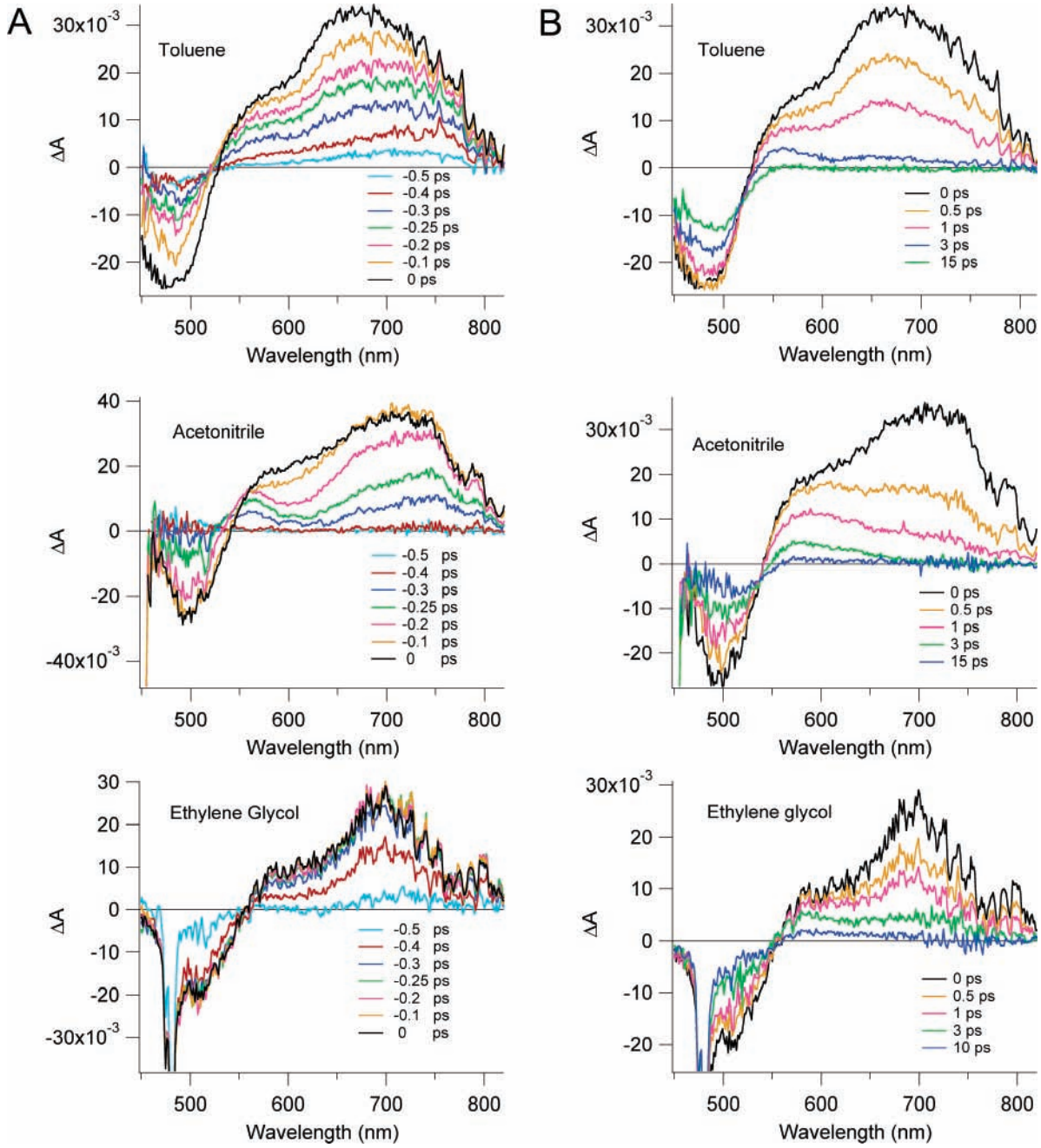

Figure 8. Transient absorption spectra at different delay times for DR1 in toluene, acetonitrile, and ethylene glycol with pump wavelengths of 425, 445, and 480 nm, respectively. (A) Early times, before the maximum of the laser pulse; (B) during decay of the excited-state population.

The value of the anisotropy $r(t,\lambda)$ depends on the angle β between the transition dipole moments of the $S_0 \rightarrow S_2(\pi\pi^*)$ transition (pump) and the transition dipole moments of the transitions probed according to eq 2.

$$r = \frac{2}{5}\left(\frac{3\cos 2\beta - 1}{2}\right) \qquad (2)$$

When $\beta = 0$, the theoretical maximum value $r = 0.4$ is found. This can be expected to be found when the same transition is probed that was pumped, that is, in the wavelength range where the ground-state absorption predominates, and for stimulated emission along the same transition. The anisotropy can decay with time due to rotation of the excited molecules, but for molecules of the size of DR1 this requires a longer time than the few picoseconds in which the excited-state population decays.

The polarization anisotropy for transient absorption of DR1 in toluene (Figure 11) is found to be only slightly dependent on the time delay after excitation: the anisotropy decay time in the range of the long-wavelength band (700 nm) is ca. 8 ps, an order of magnitude slower than the decay of the band itself (0.9 ps). For ethylene glycol no decay of polarization anisotropy was detected. For both solvents, however, the values of anisotropy are dependent on the probe wavelength (Figure 12). In the range <600 nm the anisotropy value is about 0.35, because the spectrum is dominated by transitions between S_0 and the $\pi\pi^*$ state. At longer wavelengths it gradually decreases to about 0.3 (toluene) and 0.2 (ethylene glycol) in the range of the pure low-energy band. This indicates that the angle between

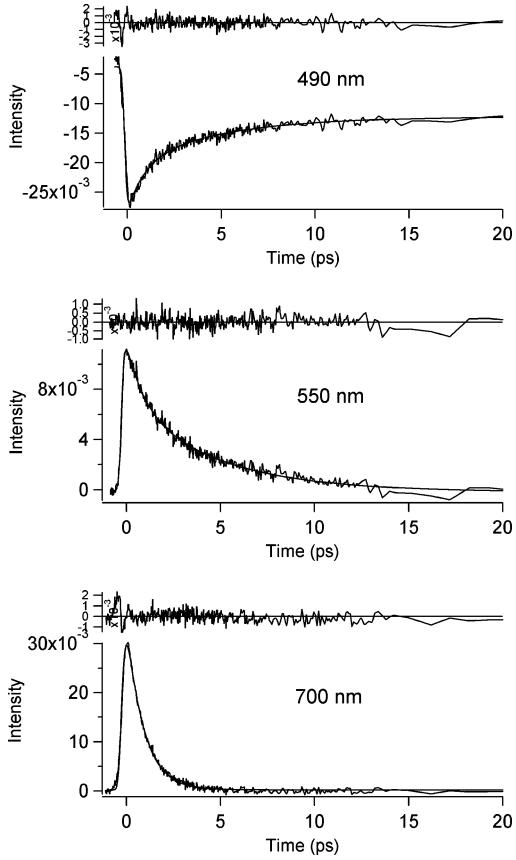

Figure 9. Kinetic traces at different wavelengths for DR1 in toluene. The best fits (see Table 4) and residual distributions are also shown.

the transition moments of the two transitions involved (pump, $S_0-\pi\pi^*$; probe, S_1-S_n) is not zero; the values of $r = 0.2$ and $r = 0.3$ correspond to angles of 24° in toluene and 17° in ethylene glycol, respectively.

Discussion

Reaction Scheme. The minimum model that can accommodate our experimental observations is depicted in Scheme 2. The excitation pulse depletes the ground state (GS), leading to a clearly reduced absorption near the GS absorption maximum. An excited state (ES) absorption band is observed, which is very broad and peaks near 700 nm. In toluene and acetonitrile the ES absorption rises slightly more slowly than the integrated system response. Simultaneously with this rise, the spectra appear to shift to the blue. Decay of the ES absorption occurs with reduction of the GS depletion, but because the ground state is vibrationally excited, its spectrum is broadened toward longer wavelengths, causing a transient absorption with a lifetime of several picoseconds near 550 nm. Formation of the photoproduct is apparent at longer times because recovery of the GS absorption near 460 nm is incomplete.

Assignment of the Excited State Absorption Band. Based on the high molar absorption coefficient of the GS absorption band (See Table 1), it is evident that excitation initially produces the $\pi\pi^*$ state, which has considerable CT character. The difference GS absorption spectrum after a nanosecond laser pulse or a lamp flash indicates that the $n\pi^*$ state is the lowest in energy, at least for the *Z* isomer. The quantum chemical calculations support the hypothesis that this is the case as well along the twisting and inversion coordinates. Thus, it is tempting to attribute the ES transient absorption band peaking near 700 nm to the $n\pi^*$ state. The ES absorption band corresponds to a

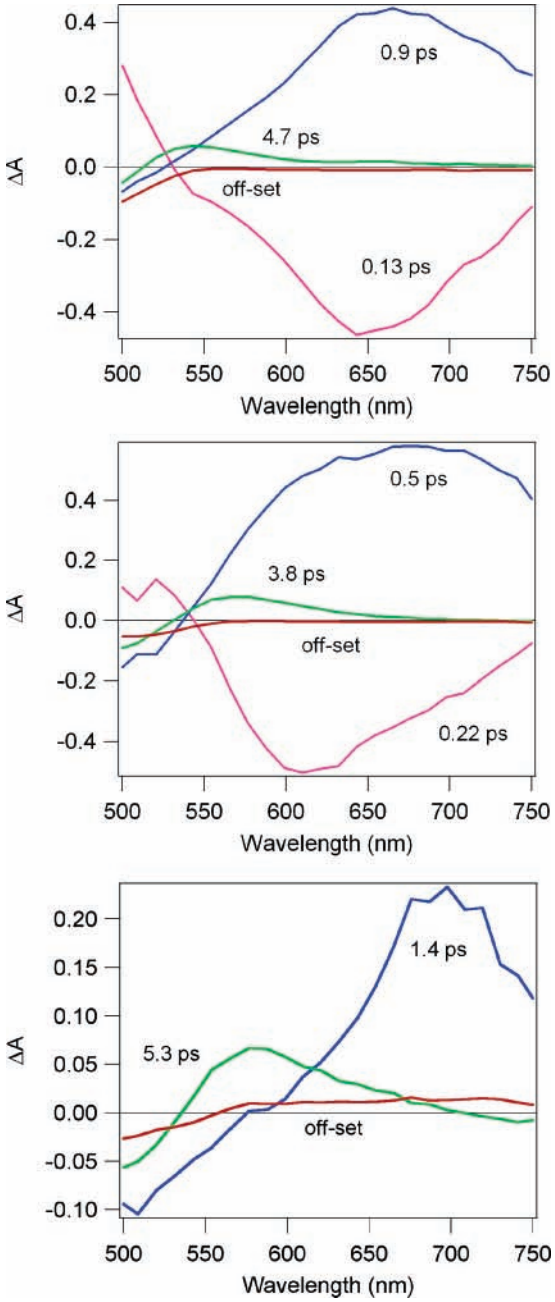

Figure 10. Results of the best global fits (decay-associated spectra) to the transient absorption data for DR1 in toluene, acetonitrile, and ethylene glycol.

strongly allowed transition, suggesting that it has $\pi-\pi^*$ character. Such transitions, however, are possible both from the $n\pi^*$ excited state and the $\pi\pi^*$ excited state. Unfortunately, it is presently not possible to perform reliable calculations of the excited state absorption spectra of molecules as complex as DR1 or DMANAB. If the ES absorption originated from the $\pi\pi^*$ state, a strong stimulated emission would be expected. Stimulated emission from the $n\pi^*$ state, on the other hand, is likely to be very weak because of the forbidden nature of the transition.

The absorption anisotropy is relatively high in the wavelength range <600 nm because the transitions probed there are in essence those of the ground state, i.e., the same as those excited by the pump pulse. The long-wavelength ES absorption band appears to have a smaller polarization, consistent with a small difference (ca. 20°) of the direction of the transition dipole moment of the transition probed from that of the $\pi-\pi^*$ transition pumped. The strength of the excited-state absorption

TABLE 4: Time Constants and Corresponding Amplitudes from Fitting the Transient Traces of DR1 in Three Solvents at Three Characteristic Wavelengths

	Toluene			
	0.13 ps	0.9 ps	4.7 ps	offset
490 nm[a]	0.51	−0.22	−0.12	−0.15
550 nm[b]	−0.18	0.38	0.43	−0.01
700 nm[c]	−0.51	0.49		
	Acetonitrile			
	0.22 ps	0.5 ps	3.8 ps	offset
500 nm[a]	0.33	−0.43	−0.15	−0.09
600 nm[b]	−0.50	0.43	0.07	
700 nm[c]	−0.33	0.67		
	Ethylene Glycol			
		1.4 ps	5.3 ps	offset
510 nm[a]		−0.47	−0.35	−0.18
600 nm[b]		0.03	0.93	0.04
700 nm[c]		1.00		

[a] Mostly ground-state depletion band. [b] Mostly hot ground-state band. [c] Pure excited state absorption band.

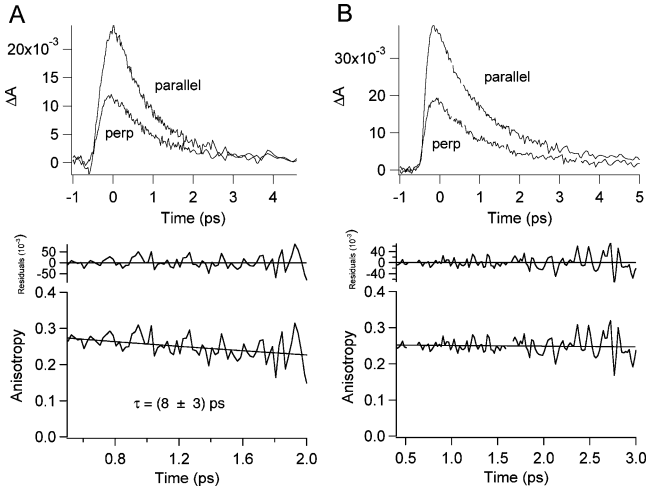

Figure 11. Transient absorption polarization anisotropy for DR1 in toluene and ethylene glycol: time dependence at 700 nm in toluene (A) and ethylene glycol (B).

indicates that it is due to a $\pi-\pi^*$ transition, which will have a transition dipole moment direction (along the long axis of the molecule) similar to that of the original absorption. The observed difference in the directions of the two transitions then points to a geometry change, which is more likely in the case of the nπ^* state.[27]

Biswas and Umapathy[12] concluded from resonance Raman experiments that the lowest excited state of DMANAB in *n*-hexane is of "locally excited" ($\pi\pi^*$) character, in benzene and more polar solvents of "charge transfer" character. According to our calculations, in addition to the nπ^* state there is only one other low-energy state, which is $\pi\pi^*$ *and* CT in nature, as illustrated in Figure 1. We suggest that the changes in the resonance Raman spectra observed by Biswas and Umapathy are due to the change in electronic structure of the $\pi\pi^*$/CT state with solvent polarity rather than a complete change in the resonant state. The nπ^* state is not observed in the resonance Raman experiments because of its low oscillator strength.

Dynamics at Very Early Times. In toluene and acetonitrile, the ES absorption band appears to rise with a time constant of 0.1−0.2 ps. This is consistent with an assignment to the nπ^* state, which has the very short-lived $\pi\pi^*$ state as its precursor.

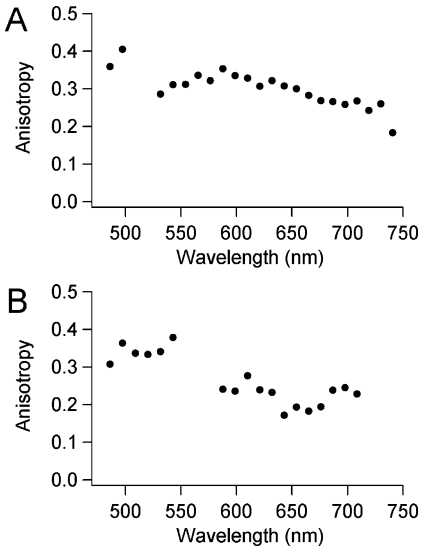

Figure 12. Wavelength dependence of transient absorption anisotropy at 0.5 ps in toluene (A) and ethylene glycol (B).

The changes in the spectral shape during the rise of the ES absorption band (Figure 8A) may be due to stimulated emission, which would be expected for the $\pi\pi^*$ state. On this time scale, however, other dynamic phenomena such as internal vibrational relaxation (as proposed by Hagiri et al.[14] for another push−pull azobenzene derivative, 4-methoxy-4′-nitroazobenzene) and solvent relaxation can cause changes in the spectral shapes with time. Solvent relaxation is likely to be more important in DR1 than in AB because of the dipolar nature of the former and the changes in dipole moments upon excitation. The reported time scale of solvent relaxation for toluene and acetonitrile[31−33] is in agreement with the time scale of the shift observed in our experiment. The S_2 state was not detected by a clear transient absorption, possibly because DR1 in this state does not absorb strongly at wavelengths within our instrumental range. A transient absorption band strongly red-shifted versus a band assigned to the S_1 state was detected in the case of AB at very early delay times by different groups[34,35] and attributed to the $S_2(\pi\pi^*)$ state of AB.

Schmidt et al.[11] recently reported time-resolved fluorescence and optical absorption measurements for DMANAB in toluene. Not surprisingly, the results of their transient absorption experiments are similar to our results for DR1 in toluene. In addition they observed a strong fluorescence with a relatively large Stokes shift immediately after photoexcitation, and a weak broad further red-shifted band during the time in which the ES absorption is present. The decay time of the strong fluorescence was similar to the rise time of the long-wavelength ES absorption. We did not observe a measurable steady-state fluorescence of DR1 in toluene or in ethylene glycol, and the weak fluorescence spectrum detected in acetonitrile was shown to be due to an impurity.

Formation of the Ground State. The transient absorption band observed near 550 nm is attributed to a hot ground state produced by the decay of the excited state. This state relaxes on a time scale of several picoseconds. At the end of this decay, a long-lived transient remains, which can be attributed to the formation of the *Z* isomer. In view of current theoretical models it is likely that both ground-state isomers are formed upon decay of the ES species to the GS PES via a conical intersection.[27,36]

Solvent Effects. The main influence of solvent polarity manifested in the DAS is a shift of the band maxima to the red and less permanent bleaching in acetonitrile and ethylene glycol

SCHEME 2

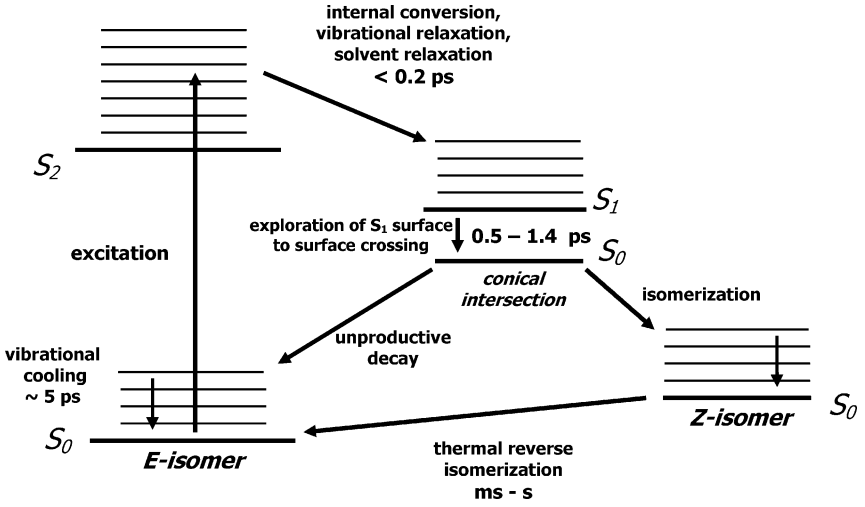

than in toluene. The first effect may be due to the fact that for DR1 the higher electronic excited states might be more polar than the nπ^* state and thus more stabilized in a polar solvent. Therefore, energy gaps between higher electronic states would become smaller, causing a shift of the spectra to the red.

A decrease in the amount of permanent bleaching with solvent polarity is indicative of lower efficiency for DR1 photoisomerization in more polar solvents. However, this cannot be quantified since both the exact spectral shapes and the absorption coefficients of the *Z* isomer in different solvents are not known. The other features of the spectra are not influenced markedly by the solvent polarity: the rise time of the ES band is comparable and the bleaching recovery is biexponential in both toluene and acetonitrile.

In the viscous and hydrogen-bond-donating solvent ethylene glycol, both positive bands have similar maxima as in acetonitrile but the ES absorption band is narrower. In ethylene glycol both bands decay more slowly than in toluene and acetonitrile and no rise of the ES absorption band can be detected. The shift of that band at early delay times is also much less pronounced. The lack of observation of a rise time in ethylene glycol may result merely from the fact that in this solvent the buildup of the ES absorption band occurs even faster than in the other solvents and therefore it is not resolved by our instrument. Possibly, the solvent polarity, and not viscosity, plays an important role in this case since the polarity of ethylene glycol is somewhat higher than the polarity of acetonitrile. It is probable that due to the solvent stabilization the energy gap between S_2 and S_1 states becomes smaller and thus the internal conversion between those two states occurs more rapidly.

The effect of solvent polarity and viscosity on the decay rate of the S_1 state cannot be mapped out completely with only three solvents. The effects do not appear to be very dramatic anyway. It is perhaps not surprising that the decay in acetonitrile is faster than that in toluene due to the smaller S_1-S_0 energy gap, while in ethylene glycol the decay is slowest, because the high viscosity slows down the exploration of the excited-state PES during the search for the conical intersection region.

Comparison with Azobenzene and Other Azobenzene Derivatives. The energy level diagram proposed in Scheme 2 for the processes occurring in the excited states of DR1 is qualitatively similar to the model reported for the parent AB and for a number of substituted derivatives. For AB itself, the kinetics are somewhat complicated. Several groups reported fast internal conversion (<0.5 ps,[35] or <0.2 ps[34]) from the $S_2(\pi\pi^*)$ state to the S_1 state. The subsequent decay of the S_1 state in this case occurs with a time constant of 0.9 ps.[34,35] Upon direct excitation to the S_1 state, however, decay is biphasic, with fast components reported as 0.1−0.3 ps in hexane depending on excitation and emission wavelength,[37] 0.3 ps in ethanol,[38] and 0.6 ps in *n*-hexane,[34] but there is also a longer component ascribed to the S_1 state, reported to be 0.6−2.0 ps (hexane, depending on excitation and emission wavelengths),[37] 2.5 ps (*n*-hexane),[34] and 2.1 ps (ethanol).[38] A longer component on the order of 10 ps observed in transient absorption is attributed to ground-state cooling. In ethylene glycol, all excited state decay processes are slower.[37,39] For 4-aminoazobenzene, in which the presence of the electron-donating amino group reduces the gap between the two lowest excited states, decay of S_2 to S_1 was reported to occur on a time scale of 0.2 ps in ethanol and heptanol, followed by a biphasic decay (0.6, 1.9 ps) from $S_1(n\pi^*)$ to the (hot) ground state.[30] Also, in 4-methoxy-4′-nitroazobenzene (MNAB) the energy gap is reduced. According to Hagiri et al.,[14] the initially prepared $S_2(\pi\pi^*)$ state (in acetonitrile) is not observed, but only the $S_1(n\pi^*)$ state, which decays in 1.2 ps, leading to a hot ground state which subsequently cools with a time constant of 3 ps. The behavior of MNAB resembles that of DR1 quite strongly. Hagiri et al. explicitly state that the spectral changes observed at early times are due to vibrational relaxation. As argued above, a contribution from stimulated emission from the S_2 state may also be responsible for the early-time spectral changes.

The kinetics of DR1 are markedly simpler than those of AB and 4-amino-AB: the transition from the initially excited $\pi\pi^*$ state occurs on a time scale <0.2 ps, similar to that in AB and several derivatives, but the decay of the nπ^* state in contrast to other cases appears a simple exponential process, even though it occurs on a time scale of only 1 ps.

The excited state absorption band, attributed to the $S_1(n\pi^*)$ state, has a somewhat lower anisotropy than the hot ground state and ground state depletion bands. In toluene a slow decay of the polarization anisotropy for the ES absorption band is observed, much slower than the population decay, but somewhat faster than what would be expected as a result of rotational motion. For AB, Chang et al.[37] attributed the anisotropy decay to large-amplitude vibrational motions which cause some reorientation of the molecules. In ethylene glycol anisotropy decay is not detected, as in AB, probably because large-amplitude motions are suppressed by high viscosity.[37]

Isomerization Pathways. Recent computational results for the parent AB clearly point to twisting of the N═N bond as the only reasonable pathway for photoinduced isomerization.[27] Our calculations of the energy gaps along the rotation and inversion coordinates confirm that the energy gap is decreased to very small values along a pure rotation coordinate, with the C−N═N bond angles staying close to 120°. This is a natural consequence of the orbital near-degeneracy caused by the effective breaking of the N═N bond. Along the inversion coordinate, the ground state maintains a closed shell character, and the gap with the S_1 state is much larger.

For thermal isomerization, the situation is less clear. Our calculations indicate that for the push−pull system it is more likely than for the parent AB that inversion occurs on the ground-state surface, but it cannot be proven that this pathway is more favorable than the N═N rotation.

Conclusions

From the GS absorption changes due to the *E*−*Z* photoisomerization, excited-state kinetics, anisotropy of the excited-state absorption, and calculations, we conclude that in DR1 push−pull substitution does not cause inversion of nπ^* and $\pi\pi^*$ states. Thus, the nπ^* state is probably the lowest excited state for this derivative, as in the parent AB.

A kinetic scheme for DR1 photoisomerization which can be derived from our experiments is similar to that proposed for AB and several derivatives. Upon excitation to the $S_2(\pi\pi^*)$ state a very fast internal conversion (<0.2 ps) to $S_1(n\pi^*)$ takes place. The S_1 state decays on a somewhat longer time scale (0.5−1.4 ps), producing a hot GS which relaxes during several picoseconds. For DR1 the latter process is slightly faster than it is for AB. In ethylene glycol the very fast component corresponding to the rise of the S_1 state was not detected, most probably due to the fact that in ethylene glycol the process occurs even faster than in the other two solvents.

The decay to the ground state occurs as a simple first-order process. For AB this is also found upon excitation to S_2, but not when the S_1 state is directly populated by optical excitation. The time constants for S_1 decay are 0.9 ps in toluene, 0.5 ps in acetonitrile, and 1.4 ps in ethylene glycol. These differences can be rationalized assuming that a polar solvent enhances the rate by reducing the energy gap and increasing the solvent reorganization energy, while the viscosity of ethylene glycol slows down the exploration of the excited-state PES during the search for a conical intersection.

The *Z* isomer is detected in the transient absorption experiments as a very long-lived transient species. It appears to be formed more efficiently in toluene than in the more polar solvents. This could not be quantified precisely because the absorption spectrum of the metastable *Z* isomer could not be determined.

Based on the literature on AB and our own calculations on 4-(dimethylamino)-4′-nitroazobenzene, it is most likely that the excited-state isomerization occurs via N═N rotation. The pathway for thermal isomerization on the ground-state surface is difficult to establish. If different reaction pathways are followed in photoisomerization and in thermal back-isomerization, this might offer an explanation for the efficiency of DR1 in light-induced matter migration, because in this case a kind of "swimming" motion could occur, rather than forward and backward movement along the same trajectory. Our calculations are not in conflict with inversion being the preferred mode of ground-state isomerization, but they cannot be considered conclusive.

Acknowledgment. This work was carried out as a part of the EC-supported project "Light-induced molecular movement" (LIMM), IST-2001-35503. We thank Michiel Groeneveld for assistence with the laser system and Emile Mes for the HPLC analysis of DR1. The computational part of this study was sponsored by the Stichting Nationale Supercomputerfaciliteiten (National Computing Facilities Foundation, NCF), with financial support from the Nederlandse Organisatie voor Wetenschappelijk Onderzoek (Netherlands Organization for Scientific Research, NWO).

References and Notes

(1) Natansohn, A.; Rochon, P. *Chem. Rev.* **2002**, *102*, 4139−4175.

(2) Landraud, N.; Peretti, J.; Chaput, F.; Lampel, G.; Boilot, J. P.; Lahlil, K.; Safarov, V. I. *Appl. Phys. Lett.* **2001**, *79*, 4562−4564.

(3) Loucif-Saïbi, R.; Nakatani, K.; Delaire, J. A.; Dumont, M.; Sekkat, Z. *Chem. Mater.* **1993**, *5*, 229−236.

(4) Buffeteau, T.; Labarthet, F. L.; Pezolet, M.; Sourisseau, C. *Macromolecules* **1998**, *31*, 7312−7320.

(5) Poprawa-Smoluch, M.; Maas, H. P. A.; De Cola, L.; Peretti, J.; Brouwer, A. M. Manuscript in preparation.

(6) Suppan, P. *J. Photochem. Photobiol., A* **1990**, *50*, 293−330.

(7) Zoon, P. D.; Brouwer, A. M. *ChemPhysChem* **2005**, *6*, 1574−1580.

(8) Zimmerman, G.; Chow, L.-Y.; Paik, U.-J. *J. Am. Chem. Soc.* **1958**, *80*, 3528−3531.

(9) Wildes, P. D.; Pacifici, J. G.; G. Irick, J.; Whitten, D. G. *J. Am. Chem. Soc.* **1971**, *93*, 2004−2008.

(10) Rau, H.; Luddecke, E. *J. Am. Chem. Soc.* **1982**, *104*, 1616−1620.

(11) Schmidt, B.; Sobotta, C.; Malkmus, S.; Laimgruber, S.; Braun, M.; Zinth, W.; Gilch, P. *J. Phys. Chem. A* **2004**, *108*, 4399−4404.

(12) Biswas, N.; Umapathy, S. *J. Raman Spectrosc.* **2001**, *32*, 471−480.

(13) Biswas, N.; Umapathy, S. *J. Chem. Phys.* **2003**, *118*, 5526−5536.

(14) Hagiri, M.; Ichinose, N.; Zhao, C. L.; Horiuchi, H.; Hiratsuka, H.; Nakayama, T. *Chem. Phys. Lett.* **2004**, *391*, 297−301.

(15) Asano, T.; Yano, T.; Okada, T. *J. Am. Chem. Soc.* **1982**, *104*, 4900−4904.

(16) Schanze, K. S.; Mattox, T. F.; Whitten, D. G. *J. Org. Chem.* **1983**, *48*, 2808−2813.

(17) Balkowski, G.; Szemik-Hojniak, A.; van Stokkum, I. H. M.; Zhang, H.; Buma, W. J. *J. Phys. Chem. A*, **2005**, *109*, 3535.

(18) *Igor Pro*, version 5.0.3; Wavemetrics, Inc.

(19) van Stokkum, I. H. M.; Larsen, D. S.; van Grondelle, R. *Biochim. Biophys. Acta: Bioenerg.* **2004**, *1657*, 82−104.

(20) van Stokkum, I. H. M.; Larsen, D. S.; van Grondelle, R. *Biochim. Biophys. Acta: Bioenerg.* **2004**, *1658*, 262.

(21) Frisch, M. J.; Trucks, G. W.; Schlegel, H. B.; Scuseria, G. E.; Robb, M. A.; Cheeseman, J. R.; Montgomery, J. A.; Vreven, T.; Kudin, K. N.; Burant, J. C.; Millam, J. M.; Iyengar, S. S.; Tomasi, J.; Barone, V.; Mennucci, B.; Cossi, M.; Scalmani, G.; Rega, N.; Petersson, G. A.; Nakatsuji, H.; Hada, M.; Ehara, M.; Toyota, K.; Fukuda, R.; Hasegawa, J.; Ishida, M.; Nakajima, T.; Honda, Y.; Kitao, O.; Nakai, H.; Klene, M.; Li, X.; Knox, J. E.; Hratchian, H. P.; Cross, J. B.; Adamo, C.; Jaramillo, J.; Gomperts, R.; Stratmann, R. E.; Yazyev, O.; Austin, A. J.; Cammi, R.; Pomelli, C.; Ochterski, J. W.; Ayala, P. Y.; Morokuma, K.; Voth, G. A.; Salvador, P.; Dannenberg, J. J.; Zakrzewski, V. G.; Dapprich, S.; Daniels, A. D.; Strain, M. C.; Farkas, O.; Malick, D. K.; Rabuck, A. D.; Raghavachari, K.; Foresman, J. B.; Ortiz, J. V.; Cui, Q.; Baboul, A. G.; Clifford, S.; Cioslowski, J.; Stefanov, B. B.; Liu, G.; Liashenko, A.; Piskorz, P.; Komaromi, I.; Martin, R. L.; Fox, D. J.; Keith, T.; Al-Laham, M. A.; Peng, C. Y.; Nanayakkara, A.; Challacombe, M.; Gill, P. M. W.; Johnson, B.; Chen, W.; Wong, M. W.; Gonzalez, C.; Pople, J. A. *Gaussian 03*, revision B.3; Gaussian, Inc.: Wallingford, Connecticut; 2003.

(22) Cossi, M.; Barone, V. *J. Chem. Phys.* **2001**, *115*, 4708−4717.

(23) Miertus, S.; Scrocco, E.; Tomasi, J. *Chem. Phys.* **1981**, *55*, 117−129.

(24) Cossi, M.; Scalmani, G.; Rega, N.; Barone, V. *J. Chem. Phys.* **2002**, *117*, 43−54.

(25) Gille, K.; Knoll, H.; Quitzsch, K. *Int. J. Chem. Kinet.* **1999**, *31*, 337−350.

(26) Gagliardi, L.; Orlandi, G.; Bernardi, F.; Cembran, A.; Garavelli, M. *Theor. Chem. Acc.* **2004**, *111*, 363−372.

(27) Cembran, A.; Bernardi, F.; Garavelli, M.; Gagliardi, L.; Orlandi, G. *J. Am. Chem. Soc.* **2004**, *126*, 3234−3243.

(28) Kikuchi, O.; Azuki, M.; Inadomi, Y.; Morihashi, K. *J. Mol. Struct. (THEOCHEM)* **1999**, *468*, 95−104.
(29) Fantacci, S.; Migani, A.; Olivucci, M. *J. Phys. Chem. A* **2004**, *108*, 1208−1213.
(30) Hirose, Y.; Yui, H.; Sawada, T. *J. Phys. Chem. A* **2002**, *106*, 3067−3071.
(31) Horng, M. L.; Gardecki, J. A.; Papazyan, A.; Maroncelli, M. *J. Phys. Chem.* **1995**, *99*, 17311−17337.
(32) Horng, M. L.; Gardecki, J. A.; Maroncelli, M. *J. Phys. Chem. A* **1997**, *101*, 1030−1047.
(33) Stratt, R. M.; Maroncelli, M. *J. Phys. Chem.* **1996**, *100*, 12981−12996.
(34) Lednev, I. K.; Ye, T. Q.; Matousek, P.; Towrie, M.; Foggi, P.; Neuwahl, F. V. R.; Umapathy, S.; Hester, R. E.; Moore, J. N. *Chem. Phys. Lett.* **1998**, *290*, 68−74.
(35) Fujino, T.; Arzhantsev, S. Y.; Tahara, T. *Bull. Chem. Soc. Jpn.* **2002**, *75*, 1031−1040.
(36) Ciminelli, C.; Granucci, G.; Persico, M. *Chem.—Eur. J.* **2004**, *10*, 2327−2341.
(37) Chang, C. W.; Lu, Y. C.; Wang, T. T.; Diau, E. W. G. *J. Am. Chem. Soc.* **2004**, *126*, 10109−10118.
(38) Nagele, T.; Hoche, R.; Zinth, W.; Wachtveitl, J. *Chem. Phys. Lett.* **1997**, *272*, 489−495.
(39) Fujino, T.; Tahara, T. *J. Phys. Chem. A* **2000**, *104*, 4203−4210.